E&G Quaternary Sci. J., 72, 37–55, 2023
https://doi.org/10.5194/egqsj-72-37-2023

Open Access E&G Quaternary Science Journal

Research article

Palaeoenvironmental research at Hawelti–Melazo (Tigray, northern Ethiopia) – insights from sedimentological and geomorphological analyses

Jacob Hardt[1], **Nadav Nir**[1], **Christopher Lüthgens**[2], **Thomas M. Menn**[3], **and Brigitta Schütt**[1]

[1]Physical Geography, Department of Earth Sciences, Freie Universität Berlin, Berlin, Germany
[2]Institute for Applied Geology, University of Natural Resources and Life Sciences, Vienna, Austria
[3]freelance archaeologist: Sanaa Branch, Orient Department, German Archaeological Institute (DAI), Berlin, Germany

Correspondence: Jacob Hardt (jacob.hardt@fu-berlin.de)

Relevant dates: Received: 24 June 2022 – Revised: 28 November 2022 – Accepted: 20 December 2022 – Published: 26 January 2023

How to cite: Hardt, J., Nir, N., Lüthgens, C., Menn, T. M., and Schütt, B.: Palaeoenvironmental research at Hawelti–Melazo (Tigray, northern Ethiopia) – insights from sedimentological and geomorphological analyses, E&G Quaternary Sci. J., 72, 37–55, https://doi.org/10.5194/egqsj-72-37-2023, 2023.

Abstract: The sites of Hawelti–Melazo in the Tigray region of the northern Ethiopian Highlands is an archaeological hotspot related to the D'mt kingdom (ca. 800–400 BCE). The existence of several monumental buildings, which have been excavated since the 1950s, underline the importance of this area in the Ethio-Sabaean period. We investigated the geomorphological and geological characteristics of the site and its surroundings and carried out sedimentological analyses, as well as direct (luminescence) and indirect (radiocarbon) sediment dating, to reconstruct the palaeoenvironmental conditions, which we integrated into the wider context of Tigray. Luminescence dating of feldspar grains from the May Agazin catchment indicate enhanced fluvial activity in the late Pleistocene, likely connected to the re-occurring monsoon after the Last Glacial Maximum (LGM). The abundance of trap basalt on the Melazo plateau, which provides the basis for the development of fertile soils, and the presumably higher groundwater level during the Ethio-Sabaean Period, provided favourable settlement conditions. The peninsula-like shape of the Melazo plateau was easily accessible only from the east and northeast, while relatively steep scarps enclose the other edges of the plateau. This adds a possible natural protective function to this site.

Kurzfassung: Die Stätte Hawelti–Melazo in Tigray im nördlichen Hochland von Äthiopien ist ein archäologischer hotspot, der im Zusammenhang mit dem Königreich D'mt steht (ca. 800–400 BCE). Seit den 1950er Jahren wurden dort mehrere Monumentalbauten entdeckt, die die Stellung dieses Gebiets zu äthiosabäischer Zeit unterstreichen. Wir haben die geomorphologischen und geologischen Eigenschaften des Gebiets untersucht, sedimentologische Analysen durchgeführt sowie direkte (Lumineszenz) und indirekte (Radiokohlenstoff) Sedimentdatierungsmethoden angewandt, um die Paläoumweltbedingungen zu rekonstruieren, die wir im weiteren Kontext von Tigray einordnen. Lumineszenzdatierungen an Feldspat-Körnern aus dem Einzugsgebiet des May Agazin deuten auf eine gesteigerte fluviale Aktivität im Spätpleistozän hin, die möglicherweise mit dem wiedereinsetzenden Monsun nach dem LGM in Verbindung steht. Der Trapp-Basalt des Melazo-Plateaus, der die Basis für die Bodenen-

twicklung bildet, und die wahrscheinlich höheren Grundwasserstände zur äthio-sabäischen Zeit boten gute Siedlungsbedingungen. Durch die halbinselartige Form des Melazo-Plateaus war es nur vom Osten und Nordosten einfach zugänglich, während die anderen Seiten des Plateaus durch steile Hänge begrenzt werden. Dies gab der Stätte eine zusätzliche natürliche Schutzfunktion.

1 Introduction

Located at the Horn of Africa, the northern highlands of Ethiopia are a region with a diverse and complex geological and archaeological history. The basaltic plateaus and the moderate subtropical climate with annual precipitation exceeding 600 mm at elevations around 2000 m a.s.l. (above sea level) provide the framework for the development of fertile soils and favourable living conditions not only throughout the Holocene. The abundance of natural resources, such as gold, obsidian, gums, incense, and more, led to the integration of this region in the ancient trade network between the Mediterranean and the Indian Ocean (Fattovich, 2012). In terms of archaeology, the area is probably best known for the Kingdom of Aksum (starting in the early first millennium CE), a state polity with the city of Aksum as its centre (French et al., 2009; Harrower et al., 2019). Prior to the Aksumite Period, the archaeological records show that groups related to the foreign Saba kingdom arrived during the first millennium BCE from the Arabian Peninsula (Japp et al., 2011; Fattovich, 2012, 2010). The most prominent remnants of this Ethio-Sabaean culture (ca. 800–400 BCE) in the present-day state of Tigray are several monumental buildings in the South Arabian style in Yeha, Wuqro, and Hawelti–Melazo, which give evidence for a complex hierarchical society and polity, which is named "D'mt" in literature (Fattovich, 2012). All of them are still being investigated or are still being excavated (Japp et al., 2011). D'mt disappears from the archaeological records at ca. 400 BCE, around the time of the decline of the Saba kingdom. The area did soon after witness the rise of the aforementioned, millennium-lasting Kingdom of Aksum (Fattovich, 2010).

Several studies investigated palaeoenvironmental changes and geomorphic activity phases in the northern Ethiopian Highlands (Tigray) and provided data to compare them to cultural epochs or relatively recent political upheavals in the region (Lanckriet et al., 2015; Nyssen et al., 2014, 2004, 2006b; Machado et al., 1998; Pietsch and Machado, 2014).

Here, we focus on the Daragá region of Tigray, which includes the archaeological sites of Hawelti–Melazo (de Contenson, 1961, 1963; Leclant, 1959) and lies within the basaltic Highlands (ca. 2000 m a.s.l.) about 10 km southeast of Aksum. Hawelti–Melazo are important Ethio-Sabaean and Aksumite find places (Menn, 2020). However, their direct surroundings have so far not been in the scope of palaeoenvironmental research. The aim of this study is to understand the late Pleistocene–Holocene environmental conditions of the area, which provided the base for the Ethio-Sabaean and the subsequent Aksumite occupations, using sedimentological analyses, luminescence and radiocarbon sediment dating methods, micromorphological analyses, and geomorphological mapping.

2 Study area

2.1 Archaeological overview

About 10 km southeast of Aksum, the archaeological sites of Hawelti–Melazo are to be found. In simplified terms, the most relevant sites are the hill of Hawelti and the so-called "plateaus" – most importantly Melazo – on the eastern banks of the river May Agazin, about 1.5 km southeast of Hawelti (Fig. 1).

The area first came into scientific consideration in the mid-1950s when a local farmer had accidentally discovered several (Ethio-Sabaean) finds at Goboshila (Melazo). This in turn led to the first excavations in Melazo, bringing to light a temple dedicated to the Sabaean god Almaqah (Leclant, 1959). Excavations continued in 1958 and 1959. On the Melazo plateau (specifically Inda Cherqos), two consecutive churches on top of each other were found, dating to Aksumite and probably medieval times – the older one incorporating spolia of Ethio-Sabaean heritage (de Contenson, 1961). Also, the stelae field on the hill of Hawelti was excavated revealing about 20 stelae, 2 buildings ("temples"), and some 500 finds (de Contenson, 1963). With regard to their dating, the results have to be considered as inconclusive since some of the features and finds are most probably from Ethio-Sabaean times (e.g. the stelae themselves), while others could be later additions. Furthermore, the interpretation of the stelae field's function remains uncertain.

Apart from minor surveys, no further investigations took place in Hawelti–Melazo until the still-ongoing Ethiopian–German cooperation project "Yeha and Hawelti–Melazo" took up work in 2009. Since then, the project has so far delivered one further major excavation site, as well as some 70 more find locations (Japp et al., 2011; Menn, 2020). Mostly, these sites and find locations point to Aksumite and Ethio-Sabaean heritage (Gerlach, 2018). While the former seem to be scattered all over the area, the latter appear to be concentrated on the hill of Hawelti and primarily the plateau of Melazo where also the excavation site is located about 60 m east of the church of Inda Cherqos. Here, a monumental building could be identified. With the construction method

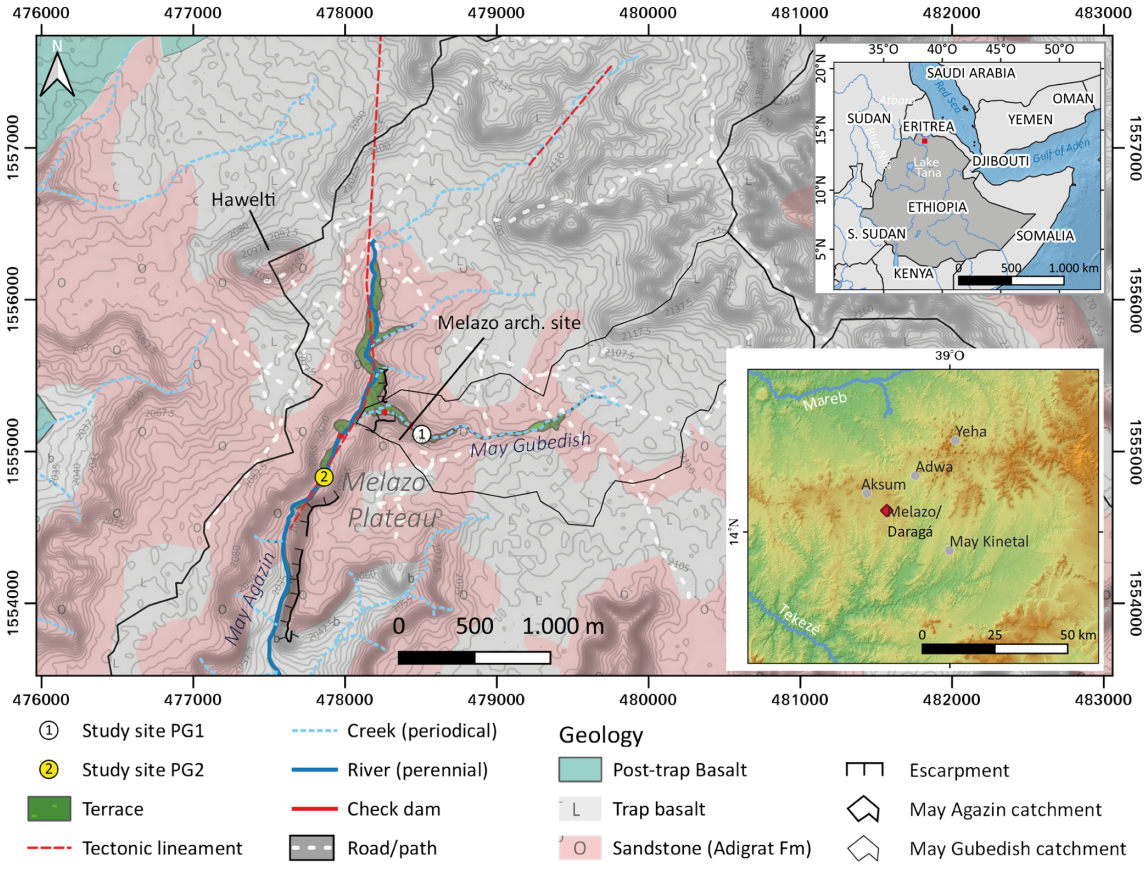

Figure 1. Geological and geomorphological map of the study area, modified from Tadesse (1999) and Hagos et al. (2010). "Melazo arch. site" refers to the location of current excavations. Several other archaeological sites were reported on the Melazo plateau to the south of the current site. Upper inset map shows the position in Ethiopia. Lower inset map shows the position in northern Ethiopia/Tigray.

similar to Yeha's Grat Be'al Gebri (Japp et al., 2011), finds corresponding to those in Yeha, and radiocarbon dating results pointing to the first half of the first millennium BCE, it can be concluded that it is of Ethio-Sabaean origin (Menn, 2020). However, several isolated finds identified during the extensive surveys also indicate the presence and possibly the settlement of people from the lithic period through to the present. Thus, the Hawelti–Melazo area has to be regarded as an archaeological hotspot.

2.2 Climate and palaeoenvironment

The study area lies in the warm and temperate subtropical highland climate zone (*Cwb* after Köppen–Geiger classification). Rainfall is mostly of monsoonal type showing a bimodal annual rainfall distribution with short rains (*belg* in Amharic) in March and long rains (*krempt* in Amharic) in June–August and a total annual precipitation of 600–700 mm (Harrower et al., 2020).

Information on late Pleistocene palaeoenvironmental conditions of the northern Ethiopian Highlands is sparse. According to Lamb et al. (2007b), Lake Tana was desiccated during the Last Glacial Maximum (LGM) due to drought caused by reduced monsoon strength (Lamb et al., 2018). A similar effect – although in a completely different environmental context – is also known for lakes in the now central Sahara (Hoelzmann et al., 2007; Umer et al., 2004). The basin of Lake Tana started to fill again at around 15 ka. In the same sense, Moeyersons et al. (2006) report increasing humidity from ca. 15 ka onwards based on numerical dating of tufa dams near Mekele (Tigray), which indicate a raised groundwater table during the late Pleistocene. Wetter conditions than today prevailed from ca. 15 ka until the mid-Holocene (ca. 5 ka; Armitage et al., 2015), owing to orbitally forced increased monsoon strength (Umer et al., 2004; Williams et al., 2006).

Climatic reconstructions for the area based on palaeopedological findings indicate that precipitation rates might have decreased in the course of the Holocene, which is in agreement with the declining monsoon strength after 5 ka (Armitage et al., 2015). Based on samples obtained close to Yeha, palaeoprecipitation rates of 870 mm a^{-1} were determined for the Early Holocene, which decreased to 780 mm a^{-1} in the first millennium BCE (Pietsch and Machado, 2014). This general trend corresponds to the find-

ings of Dramis et al. (2003), who parallelized stratigraphic sequences in Tigray with lake level records in the Rift Valley.

Machado et al. (1998) describe three "wetter" phases during the last 4000 years with enhanced soil formation, corresponding to so-called stability phases (∼ 2000–1500 BCE, 500 BCE–500 CE, 950–1000 CE), and two "drier" phases, which are represented by an increase in fluvial debris transport (1500–500 BCE, 1500–1000 CE). Lanckriet et al. (2015) compare these phases of varying morphodynamics to palaeoenvironmental studies from Lake Hayk (Lamb et al., 2007a) and Lake Ashenge (Marshall et al., 2009), as well as results from their own study site at May Tsimble (east of Mekele). This comparison confirms the general morphodynamic trends but also emphasizes several additional phases of higher and lower geomorphic activity, triggered by either climatic changes or human impact (Lanckriet et al., 2015). Human impact on the landscape in the form of land use and land cover changes comprises repeated phases of vegetation removal and intensified agriculture or livestock grazing, which have been proven throughout the last 2000–3000 years (Nyssen et al., 2004; Lanckriet et al., 2015, and references therein). Another important human imprint on the landscape are footpaths, which can incise into the land surface (Zgłobicki et al., 2021) and, for example, influence soil properties (Nir et al., 2022) and the gully erosion susceptibility (Busch et al., 2021). A footpath close to the study site was recently investigated by Nir et al. (2022) in terms of soil chemistry and micromorphology.

2.3 Geomorphological setting

The relief of the northern Ethiopian Highlands is largely structurally (tectonically and geologically) determined. Selective erosion of different rock types produced a stepped landscape, which is locally termed *amba* landscape (Coltorti et al., 2007). Several planation surfaces, the oldest being of pre-Ordovician age, once weathered and eroded at low altitudes before Cenozoic uplift of the Ethiopian Highlands, can now be found at altitudes exceeding 2000 m a.s.l. Thus, ongoing erosion not only results in stepped slopes and valleys but also exhumes relatively level palaeosurfaces (Coltorti et al., 2007; Machado, 2015).

The most typical present-day soils of the region are Vertisols and (vertic) Cambisols, which develop predominantly on the basalt surfaces and in the alluvial plains (Ferrari et al., 2015). These soils are characterized by a high content of swelling clays (montmorillonite) (Frankl et al., 2012), black colour, and relatively high fertility (Nyssen et al., 2008). Due to their high swelling potential and the seasonality of the local climate, Vertisols (locally termed *walka*; Nyssen et al., 2008) are prone to soil piping and gully erosion (Frankl et al., 2012; Nyssen et al., 2006b; Busch et al., 2021; Nir et al., 2021). Moreover, the swell-and-shrink cycles of the Vertisols trigger an upward movement of rock fragments originating from the subsurface (argillipedoturbation; Nyssen et al., 2006a).

3 Materials and methods

3.1 Fieldwork and sampling strategy

Two exposures corresponding to sections at eroded channel banks were investigated in the field and sampled for further analysis in February and November 2019. The first site in Daragá (PG1) lies on the southwestern bank of May Gubedish, a small creek flowing in a northwest direction ca. 50 m northeast of the current excavation site of Melazo. The section was chosen due to the proximity to the archaeological site, as it appeared as a potential cultural archive. The second section of Daragá (PG2) was located at the northwestern bank of May Agazin, the receiving stream of May Gubedish, ca. 300 m west of the Melazo temple and 1.5 km south of Hawelti (Table 1).

In terms of chronological control, the silty-clayey PG1 section was sampled for AMS radiocarbon dating (^{14}C), as several charcoal pieces were macroscopically visible during the sampling procedure. Oppositely, organic residue could not be found in the other sections of profile PG2, where suitable layers (sand sized, well sorted) were selected for luminescence dating. Luminescence samples were taken by driving opaque plastic cylinders (25 cm length, 5 cm diameter) into the freshly cleaned sediment, and additional samples from the bulk material were secured for radionuclide analysis.

3.2 Sedimentological analyses

The basic sedimentological analyses were performed at the physical geography laboratory of the Department of Earth Sciences, Freie Universität Berlin.

As a first preparation step, the bulk samples were dried at 105 °C, aggregates were crushed, and particles larger than 2 mm in diameter were removed by sieving. The pH values were measured with a pH meter in a solution of 10 g of dried sediment and 25 mL of 0.01 M KCl. Electrical conductivity was measured in a solution of 10 g of dried sediment in 25 mL of bi-distilled water.

The content of total carbon (TC) was determined with a Leco TruSpec CHN analyser by means of infrared CO_2 detection during sample combustion. The content of total inorganic carbon (TIC) was measured with a Woesthoff Carmhograph C-16. Total organic carbon (TOC) was subsequently calculated by the substraction of the content of TIC from the content of TC. A laser diffractometer (Beckman Coulter LS 13320) was used to determine the grain size distributions of the fractions < 1 mm. Sample preparation for grain size analysis included treatment with HCl for removal of carbonates and dispersion with sodium pyrophosphate ($Na_4P_2O_7$). Sediments from the representative units selected for dating and

Table 1. Sample overview for the studied locations.

	PG1	PG2
Location/coordinates (decimal WGS84)	May Gubedish/14.066703° N, 38.800879° E	May Agazin/14.065173° N, 38.795278° E
Bulk samples for physical and chemical analyses	27	8
Micromorphology samples	5	3
Radiocarbon samples	6 (bulk/charcoal)	/
Luminescence samples	/	2

micromorphological investigation were also mineralogically analysed by X-ray powder diffraction (XRD; Rigaku MiniFlex 600).

3.3 Micromorphological analyses

For micromorphological analyses, five sediment blocks were extracted from different sedimentary units along the profile of the main outcrop (PG1: M1–M5) and three more at sedimentary transition zones from the reference outcrop (PG2: M6_R–M8_R). Blocks were sampled using plastic boxes or jackets of gypsum bandages (plaster of Paris) depending on the sediment type and possible extraction techniques.

The micromorphological samples were dried for 4 d at room temperature (ca. 18 °C) and later heated to 50 °C for 30 h. Following this, sediments were impregnated by a 6 : 4 ($v : v$) mixture of polyester resin and acetone and a small amount of hardener (5–10 mL to 1 L of the above mixture). Due to the heavy saturation and cracking of the clay-enriched sediments, acetone removal was performed, and amounts and ratios were changed according to the reactions and impregnation of the sediments. Sampled blocks were then dried for several weeks at room temperature and cut with a slab saw to ca. 6×5 cm "hand-sized" units. These units were sent for 30 µm thick thin section preparation to Quality Thin Section Labs, Arizona. The analysis of the slides was performed applying a Zeiss polarizing microscope following a process performed by common micromorphological studies (Junge et al., 2018; Stoops, 2020; Verrecchia and Trombino, 2021).

3.4 Luminescence dating – sampling, preparation and experimental set-up, and radiocarbon dating

All preparation steps and luminescence measurements were carried out in the Vienna Laboratory for Luminescence Dating (VLL) at the University of Natural Resources and Life Sciences (BOKU) in Vienna, Austria. Sample preparation followed a standardized procedure at the VLL (Lüthgens et al., 2017; Rades et al., 2018), yielding extracts of potassium-rich feldspar and pure quartz. Samples for radionuclide determination were dried and subsequently stored in sealed Petri dishes (∼ 60 g dry weight) for at least a month to re-establish secondary secular radon equilibrium. Details on the radionuclide content and the overall dose rate calculations are provided in Table 3. All luminescence measurements were carried out on Risø TL/OSL DA-20 readers equipped with a $^{90}Sr/^{90}Y$ beta source (Bøtter-Jensen et al., 2000, 2003, 2010). Gamma spectrometry measurements for the calculation of the dose rate were performed using a Baltic Scientific Instruments (BSI) high-purity germanium (HPGe) p-type detector (∼ 52 % efficiency). The age calculation was done using the software ADELE (Kulig, 2005). Initial tests revealed very low sensitivity of the quartz in the samples, so all subsequent measurements were conducted using single aliquots of feldspar, which revealed good luminescence qualities in dose recovery experiments using a single aliquot regenerative dose protocol for the dating of feldspar (for details see Table 3). The resulting equivalent dose distributions were not significantly skewed, and average doses were calculated using the central age model (CAM; Galbraith et al., 1999). Unfortunately, only a few aliquots passed the rejection criteria for sample VLL-0492-L (for details see Table 3).

AMS radiocarbon dating was done at the Poznan Radiocarbon Laboratory. The C-14 dates were calibrated with the software OxCal v. 4.2.3 using the IntCal13 atmospheric curve (Reimer et al., 2013).

4 Results

4.1 Geomorphology

The Daragá area is situated at an elevation between 2000 and 2200 m a.s.l. within the Aksum plateau, which consists of the Oligocene trap basalts (Hofmann et al., 1997) and the Mesozoic Adigrat Sandstone (Tadesse, 1999; Hagos et al., 2010). Post-trap tectonic uplift of the region triggered extensive erosion of the flood basalts, resulting in several isolated table mountains (flat-topped mountains, locally named *ambas*) and larger plateau complexes. The plateaus are eroded by inward movement of the surrounding scarps. The inward erosion is promoted by weathering and mass wasting processes (Duszyński et al., 2019), possibly accelerated by human land

use (Nyssen et al., 2006a). The archaeological site of Melazo is situated at the southern fringe of the Aksum plateau on a peninsula-like plateau remnant corresponding to an outlier mountain (Fig. 1). The plateau remnant measures ca. 1.6 km in southwest–northeast direction and up to 600 m in the northwest–southeast direction. Its surface is flat-topped at an altitude of 2080 m a.s.l. The surrounding valley bottoms are incised up to 60 m, resulting in steep to cliff-like scarps surrounding the plateau, which expose the various colourful (reddish) facies of the Adigrat formation. To the north, the valley of May Gubedish dissects the plateau. May Gubedish is a tributary to May Agazin, which dissects the plateau on the western side. The valley of May Agazin is up to 400 m wide, and its valley cross profile ranges from an asymmetric V shape to box-like. The valley follows a tectonic lineament (Hagos et al., 2010). Alluvial plains have developed on the wide valley floors; at profile PG2, located ca. 1 km downstream of the confluence of the tributary May Gubedish, these alluvial deposits are exposed. All hydrological regimes of nearby streams are periodical (EMA map sheet 1438 D4) and recent hydraulic constructions such as weirs and check dams were installed to control the runoff (Fig. 2).

Especially to the northeast of the Melazo plateau the soil cover is thin, resulting in frequently outcropping bedrock. The area is rural with sparse settlements; basically the whole plateau is used for arable farming while the alluvial plains of the valley bottoms are used for grazing. Stone bunds separate the fields on the plateau and the slopes, acting as erosion protection measures (Fig. 2). The widespread abundance of rock fragments covering the surface of the plateau areas can be explained by argillipedoturbation, accelerated by the use of ploughs (Nyssen et al., 2002).

The catchment of May Gubedish measures 2.27 km^2. It has a length (east–west) of roughly 3 km and a width (north-northwest–south-southeast) of up to 1 km. Ca. 30 % of the catchment is grounded in Adigrat Sandstone, while the remaining 70 % of the catchment drains trap basalt. The sandstone dominates the lower section of the catchment and is found partly also in its middle reach. The whole headwater area consists exclusively of basaltic bedrock.

While flowing through basaltic bedrock the valley profile of May Gubedish corresponds to a shallow hollow valley. To the north of the Melazo plateau, entering the Adigrat Sandstone, the May Gubedish valley is incised 10 to 20 m with a now box-like valley profile. Thus, the flanks are steeper than in the upper catchment, and slope erosion is more intense. To the northeast and north of Melazo, profile PG1 is exposed at an undercut bank where the channel of May Gubedish today incises ca. 3 m into its own sediments deposited at a local valley widening upstream of a narrow point. Downstream of the narrow point the valley profile gets box-like and is infilled by alluvial deposits. The slopes flanking the channel are covered by numerous loose blocks and stone bunds stabilize the slopes where tillage occurs; gullies can be witnessed on both valley flanks frequently stabilized by check-dams.

4.2 Sedimentology and dating results

The sediment profile PG1, located at the southwestern bank of the May Gubedish creek (Fig. 2), is built of three major lithofacies units: the overlying 160 cm sediments are formed of alternating strata each with a thickness up to 15 cm, summarized as laminated sand, silt, and mud occurring alternatively with horizontally bedded sand facies (Fl/Sh). At 160–310 cm below surface, sedimentary facies are of massive mud and silt (Fm), underlain by clast-supported, horizontally stratified gravel (Gh) 310 cm below surface. The transition between the three lithofacies units takes place gradually. In total, six different sedimentary units occurring in varying thickness and frequency could be observed in the profile (Fig. 3).

Units I and V build the major part of the outcropping sediments. Units II, III, IV, and VI are coarse-grained layers of limited thickness (2–15 cm), which separate units I and V. Unit I has a dark gray-black colour and a clayey-sandy matrix containing sharp-edged gravel. It forms the main sedimentary unit of the Fl/Sh facies of the section and can only be found until a depth of 90 cm. In its uppermost part, at 0–50 cm below surface, unit I is intersected four times by unit II, a poorly sorted stone layer with a sandy-clayey matrix and a thickness of up to 10 cm; the stones have rounded edges and a diameter of 5–10 cm. Unit III is characterized by coarse gravels in a sandy-clayey matrix occurring in thicknesses of 5–10 cm, being recorded five times between 100 and 160 cm below surface. Sedimentary unit IV was recorded in six layers of up to 12 cm thickness between 40 and 90 cm below surface. It corresponds to a red-white-grayish sand layer, occasionally containing cobbles less than 3 cm in diameter. Below 90 cm depth sedimentary unit V appears, becoming the dominating sedimentary unit 160–310 cm below surface (Fm). Unit V is a gray-green massive silty clay, which is heavily compacted. Between 90 and 160 cm below surface gravel layers of unit III are repeatedly embedded into the clayey sediments of unit V. The base of the section (Gh), below 310 cm depth, is characterized by several coarse gravel and stone layers (unit VI) intercalated by unit V. Round-edged stones 15–20 cm in diameter were recorded.

The pH values across most parts of the section are rather heterogeneous and range between pH 5.9 and pH 7.1. The lowest values were measured between 170 and 220 cm below surface (pH 5.2–5.5). The electrical conductivity of the sediments ranges between 0.06 and 0.46 mS cm^{-1}. The uppermost 70 cm of the section show very low conductivity values (0.07–0.09 mS cm^{-1}). Below 70 cm depth, from top to bottom, the electric conductivity values of the sediments increase. The contents in organic (TOC) and inorganic (TIC) carbon are at a generally low level below 0.8 wt % with only minor excursions (Fig. 3).

The radiocarbon dating resulted in ages ranging from 1432 ± 85 BP (DAT4) to 4603 ± 185 BP (DAT5; Table 2). However, the ages are not in a chronostratigraphic order.

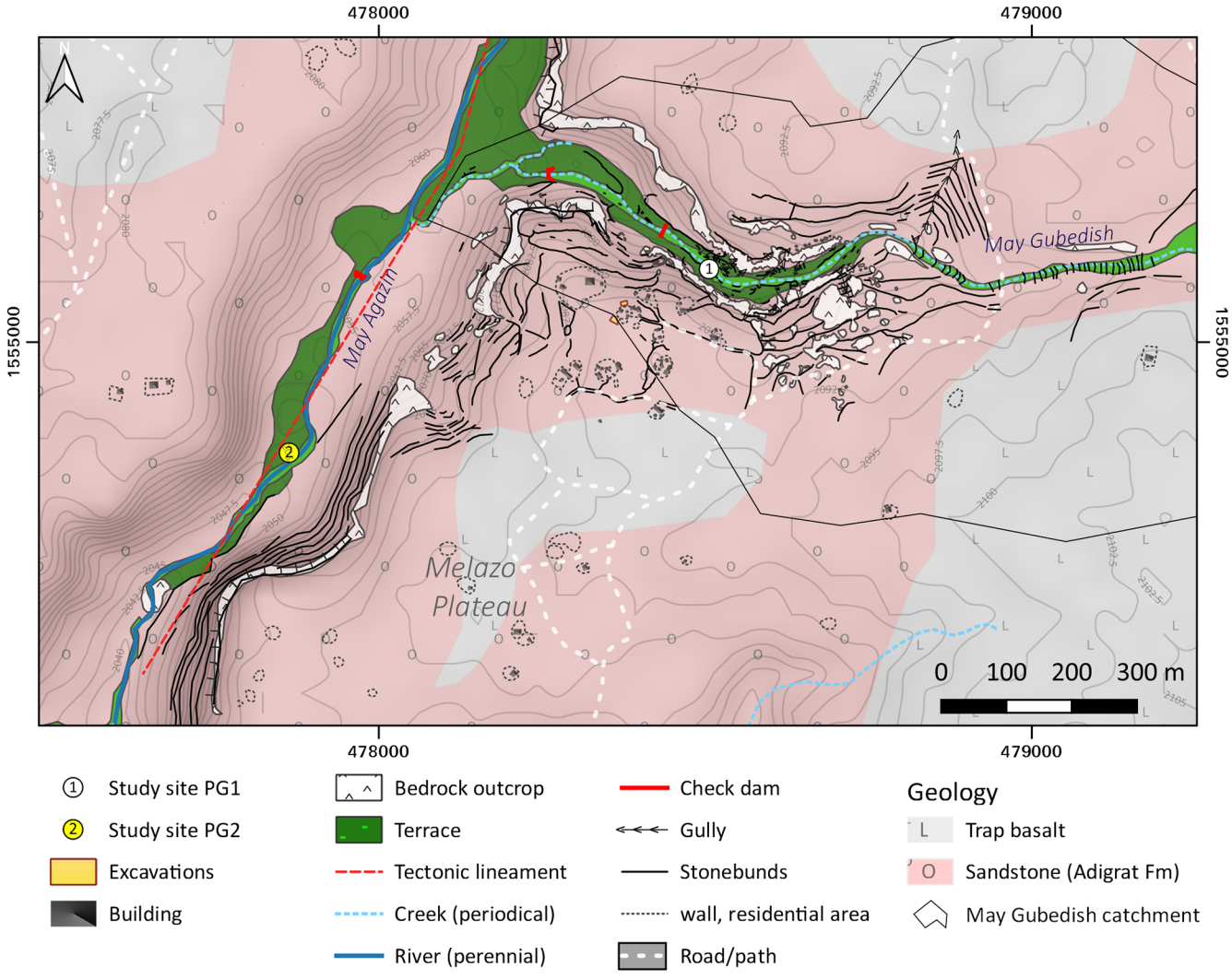

Figure 2. Geomorphological and geological map of the study area. Geology modified from Tadesse (1999) and Hagos et al. (2010). Hillshade and isolines (2.5 m spacing) based on AW3D30 digital elevation model (Jaxa, 2005).

Table 2. Overview of radiocarbon ages. All ages derived from section PG1 at May Gubedish (14.066703° N, 38.800879° E). Calibrated ages calculated using OxCal v. 4.2.3 and the IntCal13 atmospheric curve (Reimer et al., 2013). Values in bold represent the calibrated ages referred to in the text.

Lab code	Field code	Depth (cm)	Raw C-14 age BP	Calibrated age BP
POZ-126495	DAT1	65	1600 ± 30	**1470 ± 65**
POZ-114362	DAT2	70	2840 ± 360	**3021 ± 898**
POZ-123179	DAT3	100	2425 ± 30	**2525 ± 173**
POZ-123180	DAT4	180	1530 ± 30	**1432 ± 85**
POZ-126496	DAT5	365	4045 ± 35	**4603 ± 185**
POZ-122126	DAT6*	30	605 ± 30	**598 ±85**

* Sample DAT6 was taken 5 m downstream from PG1.

Sediment profile PG2, at the northwestern bank of May Agazin (Fig. 2), exposes eight strata, summarized in three different types of lithofacies: laminated sand, silt, and mud (Fl) characterize the overlying strata of the profile (0–260 cm below surface), interrupted by a layer of clast-supported, horizontally stratified gravel (Gh) 30–65 cm below surface. Below 260 cm depth lithofacies of the outcropping sediments correspond to high-energy fluvial deposits of planar-cross-bedded gravel (Gp) and planar-cross-bedded sand (Sp). The top layer (layer 1, 0–30 cm below surface) is of dark brown colour and consists of sandy silt with nested pockets filled with gravels and stones. Layer 2 (30–65 cm below surface) consists of compacted, light brown to gray silty sand with a gravelly matrix, and locally semi-angular stones are horizontally embedded. Underlying layer 3 (65–68 cm below surface) is composed of compacted brown to dark gray silt; its boundaries to the overlying layer 2 and underlying layer 4

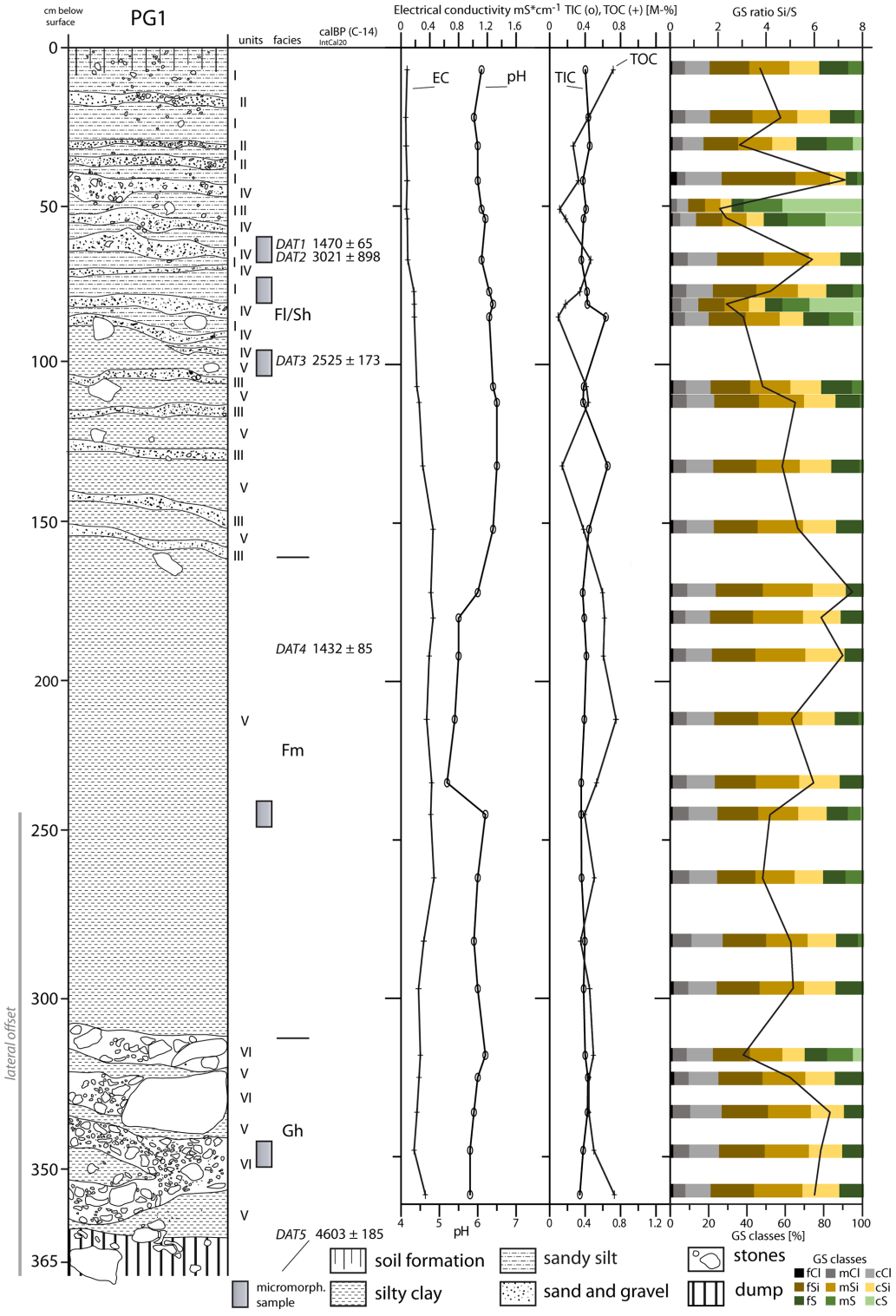

Figure 3. Sediment section PG1. Unit I: gray-black, fine roots, heavily compacted, clayey-sandy matrix with sharp-edged gravel content. Unit II: poorly sorted stone layer, 5 up to max 10 cm in diameter, rounded edges, sandy-clayey matrix. Unit III: coarse gravel layer, sandy-clayey matrix. Unit IV: red-white-grayish sand grains, occasional cobbles less than 3 cm in diameter. Unit V: gray-green massive silty clay, heavily compacted, partially embedded gravel layers (III), vertically elongated rust stains up to 1 cm length. Unit VI: gravel and stone layer. Lithofacies codes according to Miall (1996): Fm – massive mud, silt; Fl – laminated sand, silt, and mud; Sh – horizontally bedded sand; Gh – clast-supported, horizontally stratified gravel. Photographs of section PG1 can be found in the Supplement.

Table 3. Optically stimulated luminescence (OSL): results from radionuclide analysis and luminescence dating. Values in bold represent the fading corrected ages referred to in the text.

Sample lab code	Sample field code	^{238}U (Bq kg^{-1})	^{232}Th (Bq kg^{-1})	^{40}K (Bq kg^{-1})	Depth (m)	Grain size (µm)	Overall dose rate Fs (Gy ka^{-1})[a]	IR50 (n)[b]	IR50 D_e (Gy)[c]	IR50 age (ka) faded[d]	IR50 age (ka) fading corr.[e]
VLL-0491-L	PG-2-OSL5	11.18 ± 1.39	15.25 ± 1.16	200 ± 12	1.2	150–200	1.87 ± 0.15	27	23.43 ± 1.03	12.5 ± 1.1	**15.9 ± 1.5**
VLL-0492-L	PG-2-OSL6	10.80 ± 1.56	12.04 ± 0.95	127 ± 9	2.6	100–300	1.66 ± 0.13	9	25.37 ± 1.51	15.3 ± 1.5	**19.5 ± 1.5**

[a] Cosmic dose rate determined according to Prescott and Stephan (1982; Prescott and Hutton, 1994), calculated with respect to geographical position of the sampling spot (longitude, latitude, and altitude), depth below surface, and average sediment overburden density. Cosmic dose rate assigned with a 10 % error. External and internal dose rate calculated using conversion factors of Adamiec and Aitken (1998) and β attenuation factors of Mejdahl (1979), including an alpha attenuation factor of 0.08 ± 0.01, as well as an internal K content of 12.5 ± 0.5 % (Huntley and Baril, 1997) and an estimated average water content of 15 ± 5 % throughout burial time. Error was propagated to the overall dose rate calculation.

[b] Number of aliquots (4 mm diameter) passing all rejection criteria (20 % recycling ratio, 20 % recuperation in percentage of the natural signal, and 20 % test dose error, all values based on results from dose recovery experiments yielding recovery ratios in agreement with unity within error). A feldspar single-aliquot regenerative-dose (SAR) protocol using a stimulation temperature of 50 °C and a preheat temperature of 250 °C held for 60 s was used for the determination of the equivalent dose (Wallinga et al., 2000). Luminescence signals were detected through a LOT/Oriel D410/30 optical interference filter, selecting the K-feldspar emission at 410 nm (Krbetschek et al., 1997).

[c] Calculated using the CAM (Galbraith et al., 1999).

[d] Calculated using the software ADELE (Kulig, 2005).

[e] Corrected for fading according to the method of Huntley and Lamothe (2001) using the R Luminescence package (Kreutzer et al., 2012). A g value of 2.6 ± 0.3 (average value of 12 aliquots for sample VLL-0491-L) was determined using fading experiments according to Auclair et al. (2003). The fading corrected ages are used for all interpretation in this paper.

are in sharp contact. Layer 4 (68–74 cm below surface) corresponds to a light brown sandy silt in a gravelly matrix. There are several vertical cracks cutting the whole layer, which are filled with the material of layer 3. These cracks continue throughout the underlying layer 5 (74–87 cm below surface), which has a light brown colour with orange patches and consists of sandy silt with a less gravelly matrix than the above layer. It is connected with a diffuse contact to underlying layer 6 (87–97 cm below surface), a 10 cm thick layer of silt with distinct horizontal rust bands. The aforementioned cracks end in layer 6. Layer 7 (97–152 cm below surface) consists of silt and has a yellowish gray colour. Occasionally there are gravels and stones (2–4 cm in diameter) embedded. Luminescence dating of layer 7 revealed at 120 cm below surface a burial age of 15.9 ± 1.5 ka (fading corrected; see Table 3) for this layer. The exposed basal layer 8 (below 152 cm below surface) is characterized by an intercalation of several sorted sub-layers with various grain sizes; below 220 cm depth the sub-layers become bevelled. Rust and manganese bands occur occasionally. The luminescence measurements for layer 8 (260 cm below surface) yielded a depositional age of 19.5 ± 1.5 ka (fading corrected; see Table 3).

Comparable to section PG1 the pH values of the sediments in section PG2 range between pH 6.7 and pH 7.1. The highest pH value was recognized in layer 2, at a depth of ca. 50 cm. The electrical conductivity increases from ca. 0.2 mS cm^{-1} in layer 1 to the bottom, peaking in layer 4 (0.4 mS cm^{-1}). The TOC content is the highest in layer 1 (1.2 wt %) with two minor peaks in layers 3 (0.3 wt %) and 5 (0.23 wt %). Below 100 cm depth, the TOC decreases to values less than 0.2 wt %.

4.3 Micromorphology

At the May Agazin section (PG1), the groundmass is composed of silty to clayey weakly developed sub-angular blocky peds (Fig. 5a, c, d). The dominating colours are brown-gray-red with reduced grey more present at the bottom part, likely due to changes in groundwater level. Overall pedo-features are mostly in the form of organic and iron impregnations with some pedoturbation and little bioturbation. Little change is evident along the profile with Fe oxides, organic residues, and limpid clays detected along infilled channels. At 65–70 cm below surface (Fig. 5a), disordered interlayerings of coarse sands and gravel-sized grains with finer material are found at times along planar voids or infilled channels. They are mostly layered semi-diagonally at a 45–60° angle. These sub-rounded gravel-sized grains could be a result either of redeposition of fluvial sediments due to sheet erosion from the slopes or of a low-energy fluvial deposition. Sub-rounded sand-sized black metal oxide pseudomorphs are more dominant at this depth. The latter do not seem to be in situ pedo-features but oxidized and redeposited or pedoturbated within planes. At 110 cm below surface, the grey-gley colour decreases, and a brown-red Fe matrix dominates the micro-

mass, indicating either more intense oxidation, most likely due to post-depositional percolation, or the groundwater not reaching up to this level (Fig. 5b). The latter process appears to be more dominant. Voids coated or infilled with limpid clay, sand-sized minerals, and hyper-coated nodules are mostly in association with planes and suggest older plane (crack) formation and therefore several cycles of pedoturbation. This process could occur either near the surface or as result of the total de- and re-hydration of the entire soil column. Some smaller voids are more rounded than the larger ones, and chambers and vesicles are common. These features indicate bioturbation occurred or is preserved over the overlying pedoturbation on the smaller scale (20–100 µm; Fig. 5, Appendix A).

Section PG2, exposing fluvial deposits of May Gubedish, exhibits silicious cementation, as well as vertical Fe oxidized cracking (Fig. 5e, f). The three micromorphological samples taken show sand- to gravel-sized volcanic minerals along with basalt rock fragments (Fig. 5e, f, g). The gravel-sized grains are coated by clay but seem to lack silt, suggesting a surface-related process of mud drying on these grains rather than a post-depositional one. The differences between the layers are related to void sizes (compaction) and to some extent to a dominance of the clayey matrix. The layers, however, exhibit large sub-angular sand- to gravel-sized grains and occasional Fe/Mn pseudomorphs. This suggests a strictly fluvial, medium-energy deposition with very minimal post-depositional activities. At 120 cm below surface (Appendix A) sand-sized grains are deposited sub-horizontally following the inclination of the present-day surface. Iron oxide nodules are mainly ordered vertically along cracks and infilled channels while some of the grains are aggregated. These observations indicate a lower-energy deposition for layer 7 (97–150 cm) than for the lowermost layer (layer 8; Fig. 5g), with some vertical voids indicating roots and/or dehydration cracks (related to the nearby surface above) infilled with oxides. A further decrease in stream energy is evident at 68–74 cm below surface (layer 4, Fig. 4), where the groundmass is compacted, matrix supported, and dominated by clays. A post-depositional silicious cementation has likely replaced biogenic features and post-dates all other features (Fig. 5e, f).

5 Discussion

Both investigated sedimentary sections and the geomorphological mapping provide insights into the late Pleistocene–Holocene palaeoenvironmental development of the Daragá area.

At the May Agazin site (PG2), the outcropping sediments are all of fluvial origin. In the basal layer 8, the sorted sands, gravels, and pebbles indicate fluvial deposition at a point bar close to the channel under varying, but generally rather high, velocities (Pazzaglia, 2013). In the overlying layer 7, laminated sands and fine gravels indicate floodplain deposition possibly related to a shift in the meandering channel in the rather wide May Agazin valley (Hooke, 2022). Accordingly, layers 6, 5, and 4 correspond to cycles fining upwards, indicating decanted floodplain deposits (Dunne and Alto, 2013; Pazzaglia, 2013). In layers 4 and 5, organic carbon contents are slightly increased. While these increased organic carbon contents could relate to redeposited organic material on the floodplain, they might also indicate soil-forming processes in a phase of reduced flood frequency (Kennedy and Woods, 2013). This interpretation agrees with the cracks infilled with fines coated by Fe oxides pervading layers 4, 5, and 6, which are signs of desiccation at the surface (Verrecchia and Trombino, 2021). Also the presence of silicified plant material observed in layer 4 (Fig. 5e) indicates that this layer formed a surface for at least some time and possibly underwent soil-forming processes. We assume that this surface was partly eroded before the accumulation of overlying layer 3 as indicated by the sharp contact between layers 3 and 4. The minor thickness of layer 3 and its sandy character indicate a single smaller flood event (Knox and Daniels, 2002). Also in layer 3, increased organic carbon contents are taken as indicators for post-sedimentary soil development and, thus, indicate a post-sedimentary phase of low flood frequency (Dixon, 2013). In contrast, in the overlying layer 2 the 50 cm thick package of unsorted sand, gravel, and sharp-edged rocks indicates strong flood activities (Benito, 2013) possibly with material contribution from the steep surrounding slopes (Nyssen et al., 2006a). However, as there is no age control for the uppermost metre of the sediment profile, a possible connection between late Holocene human impact such as deforestation (Lanckriet et al., 2015) remains highly speculative.

The deposition of layers 8 (VLL-0492-L; 19.5 ± 1.5 ka) and 7 (VLL-0491-L; 15.9 ± 1.5 ka) falls into the LGM–late Pleistocene glacial–interglacial transition period. Within 1σ error, both ages almost overlap, and within 2σ error, both ages do overlap. Given the poor luminescence properties (dim signals) of both samples, which required 4 mm aliquots each containing several hundreds of grains to be measured, signal averaging may lead to an overestimation of the ages: the luminescence signals from well-bleached grains will be masked by the much brighter luminescence signals from older feldspar grains which were not sufficiently bleached during the last sedimentary cycle (Thrasher et al., 2009; Rhodes, 2011). This is especially true for sample VLL-0492-L, which required measuring in a very broad grain size range from 100–300 µm (compared to a grain size range of only 150–200 µm for sample VLL-0491-L). This increases the averaging effect even more because a higher number of grains is measured per aliquot, which may serve as an explanation of the age offset of the two ages. In addition, the location of the PG2 section lies in the headwater area of the May Agazin catchment, roughly 4 km away from the divide. Thus, the possible transport distances of the feldspar grains

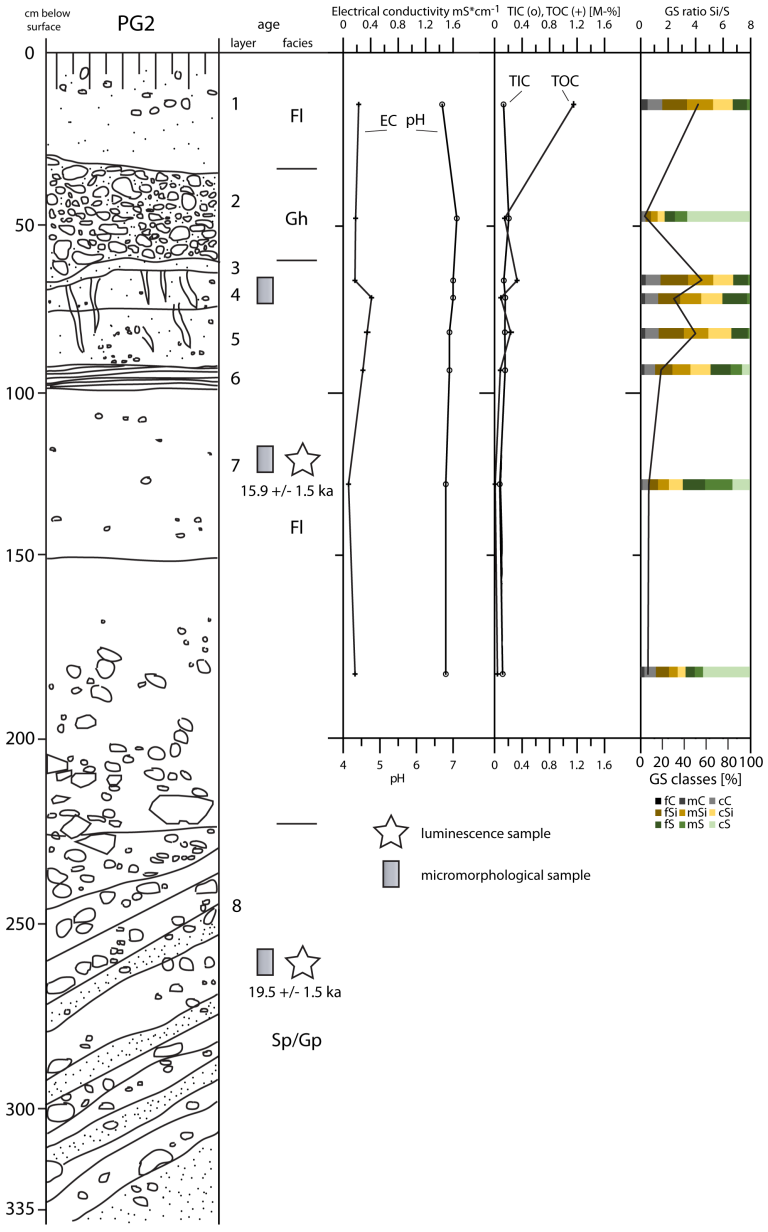

Figure 4. Sediment section PG2 (May Agazin). Layer 1: sandy silt, gravel, and stones, layered in pockets of the matrix, sub-angular small stones. Layer 2: silty sand, matrix more gravelly, rounded and semi-angular stones (2–12 cm), mostly horizontally bedded. Layer 3: sandy silt. Layer 4: sandy silt, gravels part of the matrix, sub-angular small stones. Layer 5: sandy silt with few gravels, very fine. Layer 6: silt. Layer 7: silt, occasional gravels and stones (2–4 cm), unsorted. Layer 8: intercalations of sorted layers, bedded: stones, gravels, sometimes sandy matrix. Lithofacies codes according to Miall (1996): Gp – planar-cross-bedded gravel; Sp – planar-cross-bedded sand; Gh – clast-supported, horizontally stratified gravel; Fl – laminated sand, silt, and mud. A photograph of section PG2 can be found in the Supplement.

are low, reducing the bleaching possibilities owing to only a relatively low rate of possible sedimentary cycles (Mcguire and Rhodes, 2015; Bonnet et al., 2019). Bearing in mind the possible age overestimation owing to methodological issues especially for sample VLL-0491-L, it appears more likely that both luminescence ages should be associated with the younger late Pleistocene and not with the LGM (in the case of unit 8). Consequently, both fluvial sedimentary units relate to the last glacial–interglacial transition and the abrupt onset of the summer monsoon at around ca. 15 ka (Williams et al., 2006; Gasse et al., 2008; Foerster et al., 2012). Being connected to the Nile catchment via the Tekezé and Atbara rivers, this notion is also supported by the increasing contribution of Ethiopian trap basalt components recorded in the Nile delta at the onset of the last African Humid Period (AHP) at ca. 15 ka (Revel et al., 2010; Ménot et al., 2020).

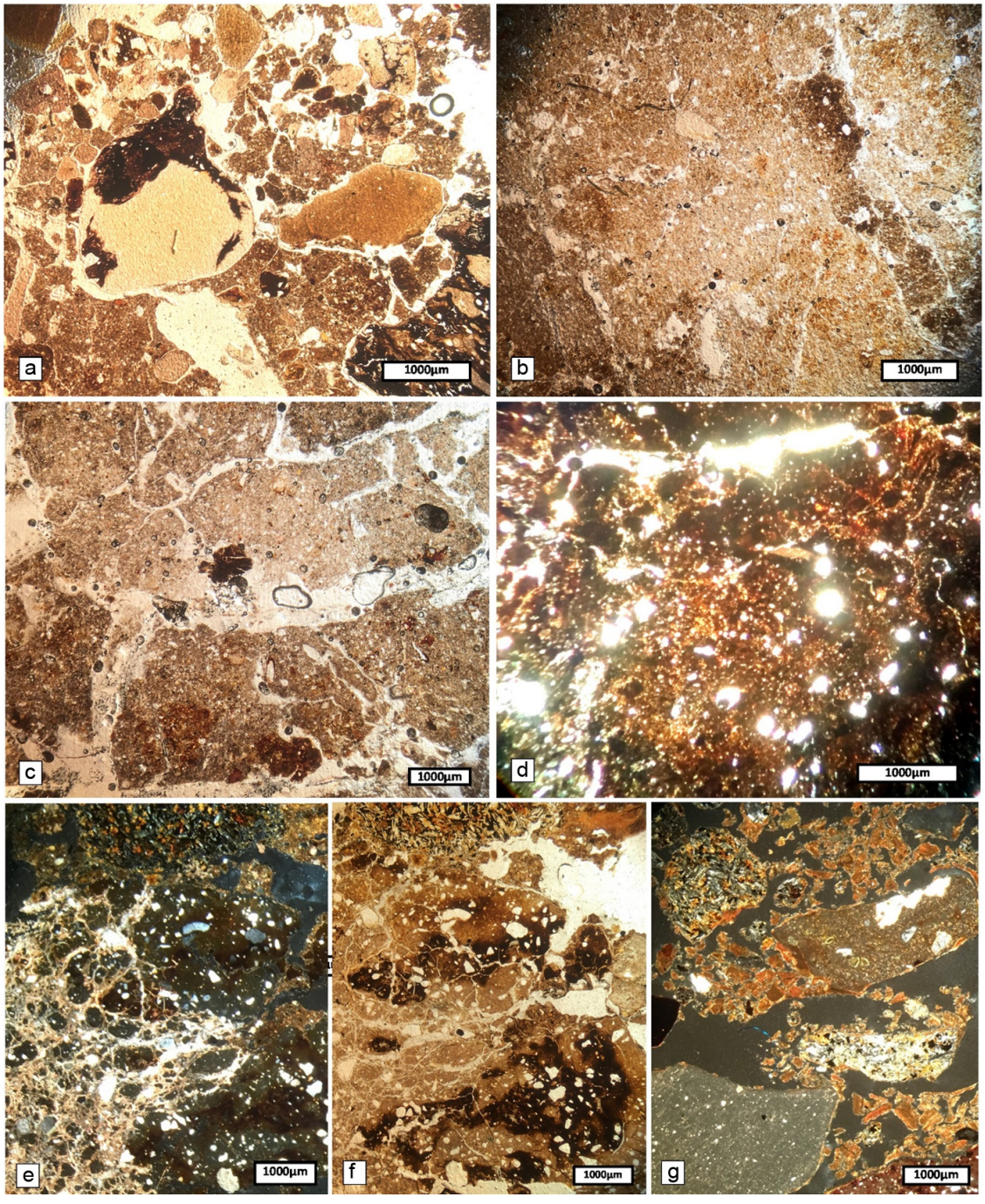

Figure 5. Thin sections of PG1 **(a–d)** and PG2 **(e–g)**. PPL = plane polarized light, and XPL = cross polarized light. **(a)** At 65–70 cm below surface (PPL) notice that the grains undergoing Mn coating are not expressed in the micromass. **(b)** At 100–110 cm below surface (PPL) clay coating and Fe–Mn oxides in a reducing and oxidizing mixed (Fe depletion) groundmass. Notice sub-vertical void along a dark brown groundmass, both typical of the matrix. **(c)** At 245–250 cm (PPL) notice that accommodating and non-accommodating planes, as well as grey and red-brown parts of the micromass, with organic impregnation and Fe–Mn oxides, are more easily differentiated. **(d)** At 365–370 cm (PPL) red-brown colour and non-accommodating planes are both more dominant. **(e)** At PG2 layer 4, 68–74 cm depth (XPL) notice that the (most likely silicious) cement is infilling voids that are cutting through the Mn–Fe oxide micromass, indicating its layer formation. **(f)** At PG2 layer 7, 115–125 cm depth: similar to panel **(e)** in PPL. **(g)** At PG2 layer 8, 255–265 cm depth (XPL) notice the basalt grain in the upper left part and limpid clay coating most of the larger grains and aggregates.

Thus, the lower parts of the PG2 section were deposited due to increased fluvial activity in response to the onset of monsoonal rainfall after a drought period during the LGM. For Lake Ashenge, Marshall et al. (2009) report increasing precipitation due to the returning monsoon already at ca. 16.2 kyr BP, which is in very close agreement with our luminescence data.

The sedimentological record from the riverbank of May Gubedish (PG1), a tributary of May Agazin, indicates completely different fluvial dynamics. The base of this section is formed by a ca. 50 cm thick package of coarse clasts (Gh facies) indicating deposition in the channel under conditions of high stream energy (Pazzaglia, 2013). The whole overlying lithostratigraphic unit (Fm facies) is dominated by silty-clayey deposits, which are in its upper layers horizontally streaked with coarser, sandy-gravelly layers (Fl/Sh facies). Either these deposits are indicative of deposition in a still water body (Reeves, 1968) or they correspond to alluvial deposits on a floodplain under very low stream energy (Pazzaglia, 2013). Deposition in a stagnant water body would require a damming situation downstream of the section, which could have been caused by a local rockfall or landslide along the river banks (Korup, 2013). The outcropping sandstone of the Adigrat Formation along the steep valley flanks and the apparent signs of ongoing gravitational mass movements at the slopes affirm this assumption (Fig. 2). Nyssen et al. (2006a) identified rockfall as an important geomorphic process in the northern Ethiopian highlands, most recently often triggered by livestock trampling. At present, however, no geomorphological evidence of a natural damming situation due to mass movements could be observed along the valley floor. The parent material of the silty-clayey deposits is the weathered trap basalt, which makes up a large part of the May Gubedish catchment (Fig. 2). The repeated occurrence of thin (few centimetres) sand and gravel layers may represent stronger rainfall events triggering slope wash and increased discharge (Cammeraat, 2013). The large clasts, which at times are embedded into the silty-clayey layers, were most likely laterally washed in from the adjacent slopes. Within the silty-clayey parts of the section signs of stratification are lacking due to pedoturbation caused by dry–wet cycles starting from the surface and influenced by a periodically alternating water table level. Consequently, Fe reduction–oxidation cycles, organic decomposition, and clay-bound swell-and-shrink processes were identified in the micromorphological analyses. The process of argillipedoturbation, which causes intense turbation of the material, has been described for Vertisols in Tigray before (Nyssen et al., 2002, 2006a). However, the sand and gravel layers above ca. 160 cm below surface have visibly not been incorporated in the pedoturbation process. Thus, we conclude that pedoturbation has not affected the larger grains and in general has mostly occurred prior to their deposition. Generally, planes and other void types are smaller than the gravels and sands in this unit and are not infilled by organic or Fe oxides as is the case for much of the lower section or even a few of the layers in this unit; i.e. gravel-sized pedomorphic organic features may have been transported within a layer in the unit but not between layers (Fig. 5).

For C-14 dating, bulk soil organic carbon was used and, thus, should be treated with caution, as soil organic carbon can be redeposited several times (e.g. old wood effect) and re-precipitate or move vertically owing to pedo- or bioturbation (Sloss et al., 2013). Our dates therefore should reflect a general time frame for the accumulation of the PG1 profile using different stratigraphic constraints to interpret the accuracy of these dates. A C-14 date from the lower part of this profile (DAT5: 4603 ± 185 BP) reveals that the early accumulation of the coarse, clast-rich Gh facies likely took place during or after the mid-Holocene. From the fines of the Fm facies, one sample was derived (DAT4: 1432 ± 85 BP), and from the layered Fl/Sh facies, three samples for C-14 dating were extracted from gravel layers (DAT1: 1470 ± 65 BP; DAT2: 3021 ± 898 BP; DAT3: 2525 ± 173 BP). Even including an age inversion due to pedoturbation, these dates indicate that sedimentation took place during the first millennium BCE and the first millennium CE; thus, it temporally corresponds to the Ethio-Sabaean and Aksumite material cultures (Phillipson, 2012). An additional date was derived from a sediment sample taken 5 m downstream of the PG 1 profile (DAT6: 598 ± 53 BP) from silty-clayey deposits (Fm facies) at a depth of 30 cm, which represents a younger reaccumulation of the May Gubedish, probably as a lower terrace segment. This age provides a frame for the incision of the May Gubedish river into its infilled valley floor, forming a river terrace that today forms the surface of PG1, which consequently took place after 598 ± 53 BP. This is in agreement with the conclusions of Lanckriet et al. (2015), who report increased channel incision especially in recent and subrecent times due to strongly increased surface runoff as a result of strong deforestation. Two C-14 outliers are likely due to syn- and post-depositional processes. Within the gravel layer DAT2 was dated 500 years older than the 50 cm deeper sample of DAT3 but with the error range of 898 years, overlapping with DAT3. However, one substantial outlier (DAT4) within the well-pedoturbated material at 1 m below this unit falls into the middle of the first millennium CE, still confirming the general age of the deposition to the late Holocene but contradicting the three ages above. This C-14 outlier is likely a result of roots activities or pedoturbation below the horizontal gravel layer. The maximum age for the deposition of the upper 180 cm of the PG1 section falls into the time of or after the decline of the Aksumite Empire (ca. 1400–1000 CE) (Phillipson, 2012), when the geomorphic activity was high due to intensified agriculture and increasing deforestation under comparably drier climatic conditions (Fig. 6; Lanckriet et al., 2015; Darbyshire et al., 2003; Machado et al., 1998).

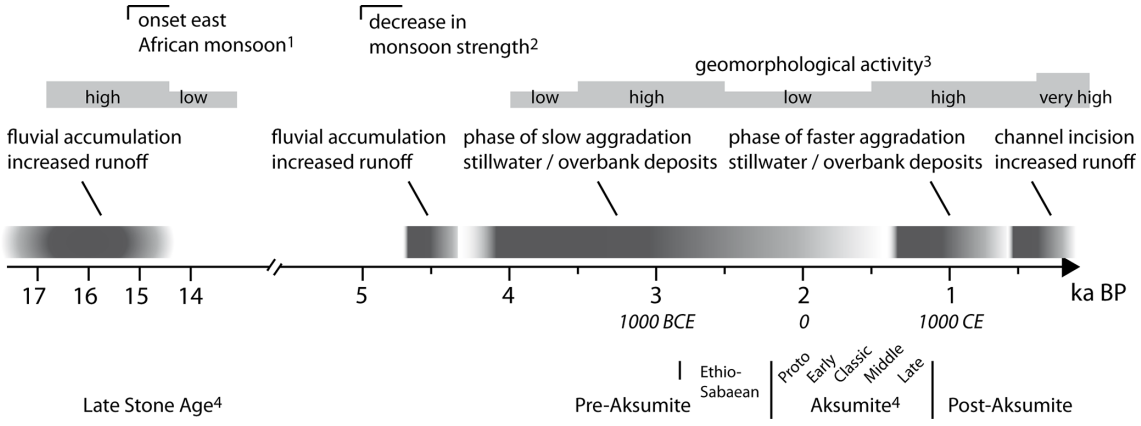

Figure 6. Integration of our results in an environmental and cultural context of northern Ethiopia. 1: Moeyersons et al. (2006), Lamb et al. (2007b), Umer et al. (2004). 2: Armitage et al. (2015). 3: this study and Lanckriet et al. (2015). 4: Bard et al. (2014), Fattovich (2012).

6 Conclusions

The environmental conditions on and around the Melazo plateau were favourable during the time of the Ethio-Sabaean settlement. This is also reflected in the findings of monumental buildings from this period. The landscape of the May Gubedish valley close to the Melazo archaeological site probably looked different during the Ethio-Sabaean period than today. The groundwater level was presumably higher, and water in the valley was probably easier to access than today due to less relief as May Gubedish was flowing at a higher level than today in its own sediments at the valley floor. Also the geological conditions appear favourable: the omnipresent Adigrat Sandstone provides building material, which is also used today for building walls and other structures. The trap basalt, found in the inner part of the Melazo plateau and the surrounding plateaus, provides fertile soils. Beyond, the peninsula-like Melazo plateau has a strong protective function as it is only easily accessible from the east–northeast, while in all other directions steep scarps enclose the plateau. The resulting large viewshed of the Melazo plateau also had tactical advantages as it allowed visitors to be recognized at an early stage. The landscape of the much wider May Agazin valley, however, was probably rather similar to most recent conditions. May Agazin like today was a hindrance for traffic, and during rainy seasons the channel could probably only be crossed at dedicated, and thus easy to control, places.

Our study provides evidence for increased fluvial activity in the May Agazin during the late Pleistocene, which is probably related to the re-occurrence of the monsoonal rainfall after the LGM. In the May Gubedish valley, being a tributary to the valley of May Agazin, coarse fluvial sediments indicating high-energy fluvial dynamics at the base of the channel were deposited around the transition from the middle to late Holocene. During the Ethio-Sabaean and probably early Aksumite period slow aggradation of the valley floor started with most likely increasing depositional rates during the late and post-Aksumite period. Since medieval or subrecent times the channel of May Gubedish incised into its own valley floor sediments – exposing the sediments of PG1 and forming a terrace which today is used for an orchard. These observations generally correlate with other studies on geomorphic activity phases in Tigray.

Appendix A

Table A1. Sedimentary analysis of selected depositional units in the PG1 and PG2 profiles. Grain sizes used are gravel (g), coarse sand (cs), medium sand (ms), fine sand (fs), silt, and clay. Sediment grain size categories are based on laser grain size analysis, while mineral occurrence is interpreted from XRD spectra. Micromass structure, mineral shapes and sizes (for those also visually identified), and pedo-features were obtained through micromorphological observation.

Site	Depth (cm)	Unit	Grain size and structure	Dominant minerals (ordered by abundance)	Pedo-features
PG1	30	Young accumulation	Clay. Weakly developed sub-angular blocky and crumble porous peds	Quartz: sub-angular (ms-fs); kaolinite, muscovite, and chlorite (silt-clay); feldspars (fs-silt); rosenhahnite	Iron mottling. Large accommodating planes and aggregates
	65–70	I/IV	Loam. Weakly developed sub-angular blocky peds, poor sorting, few sub-horizontal grain-supported layers of g-cs-sized grains	Quartz (cs-fs, sub-rounded larger grains to sub-angular smaller grains), kaolinite, muscovite, and chlorite: mostly as coating (fs-clay); plagioclase feldspar (fs); pyroxene: weathered (cs-fs) very rare	Iron mottling, organic impregnation, Mn–Fe pseudomorphs (g-ms), planes
	75–79	I/IV	Loam. Planes – ms sized in width. Moderately developed sub-angular blocky peds, poor sorting	Quartz (g-fs, sub-angular), kaolinite, muscovite, and chlorite: mostly as coating (fs-clay); plagioclase feldspar (fs); pyroxene: weathered (g-cs-fs) very rare	Some planes are infilled by the coarser material including aggregates and pseudomorphs
	95–111	V	Silty clay loam. Sub-angular blocky peds, weakly developed in a massive microstructure	Quartz mostly elliptic shaped (cs-fs); plagioclase feldspar and pyroxene: sub-angular to sub-rounded (fs); kaolinite, muscovite, and chlorite: mostly as coating (silt-clay); rosenhahnite	Iron mottling and organic impregnation, accommodating and non-accommodating planes. Voids are coated and some infilled by limpic clay and Fe–Mn oxides. Cs-sized grains are associated with planes
	345–350	V/VI	Silty loam. Weakly developed peds with poor sorting and open grain-supported structured cs-g grains at the lower part of the groundmass	Quartz: sub-angular (ms-fs), feldspar (fs-silt), kaolinite, muscovite, and chlorite (silt), possible rosenhahnite	Brown micromass with iron mottling and organic impregnation. Bioturbation is slightly more evident from the impregnation of oxides, and limpid clays feature also along infilled channels
PG2	65–68	3	Loamy sand, blocky and moderately developed peds	Quartz: sub-rounded (cs-fs); basalt: sub-angular (g-cs); clinopyroxene: sub-rounded (fs); olivine: (silt) rare; orthopyroxene: (fs) rare	Planar voids coated and filled with clays or larger grains
	68–74	4	Sandy loam, blocky in a poorly to moderately developed peds structure	Quartz: sub-rounded (ms-fs); clinopyroxene: sub-rounded (fs); basalt: sub-angular (cs) rare	Cemented by amorphous silica. Rare (g) size orthopyroxene grains with surrounding constrained minerals (corona texture) – geological feature
	97–152	7	Loamy sand with structural and planar voids. Large grains (cs-g) are crossing sub-horizontally	Basalt: sub-rounded (g-ms); pyroxene: sub-angular to sub-rounded (cs-fs); olivine: (ms-fs) rare; kaolinite, muscovite: coating (clay)	Clay coating on most of the sand-sized grains. Many of the large grains are aggregates. Mn–Fe oxide nodules (pseudomorphs) are also found along vertical lines (cracks)
	152–335	8	Sandy gravel dominant in open grain-supported structure	Quartz: sub-rounded (cs-fs); pyroxene: sub-rounded to sub-angular (ms-fs); basalts: sub-rounded (g-ms)	Three sub-units with g- and s-sized grains: 1. in large voids, 2. dominant clay-coating and 3. combination of (1) and (2) Mn–Fe oxides pseudomorphs (cs-ms) and Fe mottling. Depositional cycles

Data availability. The basic luminescence data are included in this publication. Additional data can be provided by the corresponding author upon request.

Supplement. The supplement related to this article is available online at: https://doi.org/10.5194/egqsj-72-37-2023-supplement.

Author contributions. This study was conceptualized by JH, NN, and BS, who also carried out the field work. JH and NN prepared the original draft of the manuscript. NN carried out the micromorphological analyses. CL conducted the luminescence analyses. TM provided the archaeological background. All authors discussed the results and contributed to various stages in the writing process of this paper, including reviewing and editing.

Competing interests. At least one of the (co-)authors is a member of the editorial board of *E&G Quaternary Science Journal*. The peer-review process was guided by an independent editor, and the authors also have no other competing interests to declare.

Disclaimer. Publisher's note: Copernicus Publications remains neutral with regard to jurisdictional claims in published maps and institutional affiliations.

Special issue statement. This article is part of the special issue "Quaternary research from and inspired by the first virtual DEUQUA conference". It is a result of the vDEUQUA2021 online conference in September/October 2021.

Acknowledgements. The authors wish to thank Silvan Schmieg and Robert Busch (Freie Universität Berlin) and Kristina Pfeiffer, Victoria Grünberg, Mike Schnelle, Sarah Japp, and Iris Gerlach (German Archaeological Institute (DAI), Sanaa Branch of the Orient Department). Thanks to Mareike Stahlschmidt for guidance in the analysis of the thin sections. We want to thank the two anonymous reviewers for their constructive reviews of this work.

Financial support. This research has been supported by the Deutsche Forschungsgemeinschaft (DFG) within the framework of the SPP 2143 Entangled Africa – Project Routes of Interaction (grant no. 404354728).

We acknowledge support from the Open Access Publication Initiative of Freie Universität Berlin.

Review statement. This paper was edited by Julia Meister and reviewed by two anonymous referees.

References

Adamiec, G. and Aitken, M.: Dose-rate conversion factors: update, Ancient TL, 16, 37–50, 1998.

Armitage, S. J., Bristow, C. S., and Drake, N. A.: West African monsoon dynamics inferred from abrupt fluctuations of Lake Mega-Chad, P. Natl. Acad. Sci. USA, 112, 8543–8548, https://doi.org/10.1073/pnas.1417655112, 2015.

Auclair, M., Lamothe, M., and Huot, S.: Measurement of anomalous fading for feldspar IRSL using SAR, Radiat. Meas., 37, 487–492, https://doi.org/10.1016/S1350-4487(03)00018-0, 2003.

Bard, K. A., Fattovich, R., Manzo, A., and Perlingieri, C.: The chronology of Aksum (Tigrai, Ethiopia): a view from Bieta Giyorgis, Azania, 49, 285–316, https://doi.org/10.1080/0067270X.2014.943484, 2014.

Benito, G.: 13.15 Hazardous Processes: Flooding, in: Treatise on Geomorphology, edited by: Shroder, J. F., Academic Press, San Diego, 243–261, https://doi.org/10.1016/B978-0-12-374739-6.00363-8, 2013.

Bonnet, S., Reimann, T., Wallinga, J., Lague, D., Davy, P., and Lacoste, A.: Landscape dynamics revealed by luminescence signals of feldspars from fluvial terraces, Scientific Reports, 9, 8569, https://doi.org/10.1038/s41598-019-44533-4, 2019.

Bøtter-Jensen, L., Bulur, E., Duller, G. A. T., and Murray, A. S.: Advances in luminescence instrument systems, Radiat. Meas., 32, 523–528, https://doi.org/10.1016/S1350-4487(00)00039-1, 2000.

Bøtter-Jensen, L., McKeever, S. W. S., and Wintle, A. G.: Optically Stimulated Luminescence Dosimetry, Elsevier, 355 pp., https://doi.org/10.1016/B978-0-444-50684-9.X5077-6, 2003.

Bøtter-Jensen, L., Thomsen, K. J., and Jain, M.: Review of optically stimulated luminescence (OSL) instrumental developments for retrospective dosimetry, Radiat. Meas., 45, 253–257, https://doi.org/10.1016/j.radmeas.2009.11.030, 2010.

Busch, R., Hardt, J., Nir, N., and Schütt, B.: Modeling Gully Erosion Susceptibility to Evaluate Human Impact on a Local Landscape System in Tigray, Ethiopia, Remote Sensing, 13, 2009, https://doi.org/10.3390/rs13102009, 2021.

Cammeraat, E. L. H.: 7.33 Semiarid Hillslope Processes, in: Treatise on Geomorphology, edited by: Shroder, J. F., Academic Press, San Diego, 355–362, https://doi.org/10.1016/B978-0-12-374739-6.00184-6, 2013.

Coltorti, M., Dramis, F., and Ollier, C. D.: Planation surfaces in Northern Ethiopia, Geomorphology, 89, 287–296, https://doi.org/10.1016/j.geomorph.2006.12.007, 2007.

de Contenson, H.: Les fouilles à Haoulti-Melazo en 1958, Annales d'Ethiopie, 4, 39–60, 1961.

de Contenson, H.: Les fouilles de Haoulti en 1959 – Rapport préliminaire, Annales d'Ethiopie, 5, 41–86, 1963.

Darbyshire, I., Lamb, H., and Umer, M.: Forest clearance and regrowth in northern Ethiopia during the last 3000 years, Holocene, 13, 537–546, https://doi.org/10.1191/0959683603hl644rp, 2003.

Dixon, J. C.: 4.3 Pedogenesis with Respect to Geomorphology, in: Treatise on Geomorphology, edited by: Shroder, J. F., Academic Press, San Diego, 27–43, https://doi.org/10.1016/B978-0-12-374739-6.00058-0, 2013.

Dramis, F., Umer, M., Calderoni, G., and Haile, M.: Holocene climate phases from buried soils in Tigray (northern

Ethiopia): comparison with lake level fluctuations in the Main Ethiopian Rift, Quaternary Res., 60, 274–283, https://doi.org/10.1016/j.yqres.2003.07.003, 2003.

Dunne, T. and Aalto, R. E.: 9.32 Large River Floodplains, in: Treatise on Geomorphology, edited by: Shroder, J. F., Academic Press, San Diego, 645–678, https://doi.org/10.1016/B978-0-12-374739-6.00258-X, 2013.

Duszyński, F., Migoń, P., and Strzelecki, M.C.: Escarpment retreat in sedimentary tablelands and cuesta landscapes – Landforms, mechanisms and patterns, Earth-Sci. Rev., 196, 102890, https://doi.org/10.1016/j.earscirev.2019.102890, 2019.

Fattovich, R.: The Development of Ancient States in the Northern Horn of Africa, c. 3000 BC–AD 1000: An Archaeological Outline, J. World Prehist., 23, 145–175, https://doi.org/10.1007/s10963-010-9035-1, 2010.

Fattovich, R.: The northern Horn of Africa in the first millennium BCE: local traditions and external connections, Rassegna di Studi Etiopici, 4, 1–60, 2012.

Ferrari, G., Ciampalini, R., Billi, P., and Migoń, P.: Geomorphology of the Archaeological Area of Aksum, in: Landscapes and Landforms of Ethiopia. World Geomorphological Landscapes, edited by: Billi, P., Springer, Dordrecht, 147–161, https://doi.org/10.1007/978-94-017-8026-1_7, 2015.

Foerster, V., Junginger, A., Langkamp, O., Gebru, T., Asrat, A., Umer, M., Lamb, H. F., Wennrich, V., Rethemeyer, J., Nowaczyk, N., Trauth, M. H., and Schaebitz, F.: Climatic change recorded in the sediments of the Chew Bahir basin, southern Ethiopia, during the last 45,000 years, Quatern. Int., 274, 25–37, https://doi.org/10.1016/j.quaint.2012.06.028, 2012.

Frankl, A., Poesen, J., Deckers, J., Haile, M., and Nyssen, J.: Gully head retreat rates in the semi-arid highlands of Northern Ethiopia, Geomorphology, 173–174, 185–195, https://doi.org/10.1016/j.geomorph.2012.06.011, 2012.

French, C., Sulas, F., and Madella, M.: New geoarchaeological investigations of the valley systems in the Aksum area of northern Ethiopia, CATENA, 78, 218–233, https://doi.org/10.1016/j.catena.2009.02.010, 2009.

Galbraith, R. F., Roberts, R. G., Laslett, G. M., Yoshida, H., and Olley, J. M.: Optical dating of single and multiple grains of quartz from Jinmium rock shelter, Northern Australia: Part I, experimental design and statistical models, Archaeometry, 41, 339–364, https://doi.org/10.1111/j.1475-4754.1999.tb00987.x, 1999.

Gasse, F., Chalié, F., Vincens, A., Williams, M. A. J., and Williamson, D.: Climatic patterns in equatorial and southern Africa from 30,000 to 10,000 years ago reconstructed from terrestrial and near-shore proxy data, Quaternary Sci. Rev., 27, 2316–2340, https://doi.org/10.1016/j.quascirev.2008.08.027, 2008.

Gerlach, I.: Zum äthio-sabäischen Kunsthandwerk des frühen 1. Jahrtausends v. Chr., in: Hauptsache Museum – Der alte Orient im Fokus – Festschrift für Ralf-B. Wartke, edited by: Marzahn, J. and Pedde, F., marru – Studien zur Vorderasiatischen Archäologie, 229–252, ISBN 978-3-96327-036-9, 2018.

Hagos, M., Koeberl, C., Kabeto, K., and Koller, F.: Geochemical characteristics of the alkaline basalts and phonolite-trachyte plugs of the Axum area, northern Ethiopia, Austrian J. Earth Sc., 103, 153–170, 2010.

Harrower, M. J., Dumitru, I. A., Perlingieri, C., Nathan, S., Zerue, K., Lamont, J. L., Bausi, A., Swerida, J. L., Bongers, J. L., Woldekiros, H. S., Poolman, L. A., Pohl, C. M., Brandt, S. A., and Peterson, E. A.: Beta Samati: discovery and excavation of an Aksumite town, Antiquity, 93, 1534–1552, https://doi.org/10.15184/aqy.2019.84, 2019.

Harrower, M. J., Nathan, S., Mazzariello, J. C., Zerue, K., Dumitru, I. A., Meresa, Y., Bongers, J. L., Gebreegziabher, G., Zaitchik, B. F., and Anderson, M. C.: Water, Geography, and Aksumite Civilization: The Southern Red Sea Archaeological Histories (SRSAH) Project Survey (2009–2016), Afr. Archaeol. Rev., 37, 51–67, https://doi.org/10.1007/s10437-020-09369-8, 2020.

Hoelzmann, P., Gasse, F., Dupont, L., Salzmann, U., Staubwasser, M., Leuschner, D., and Sirocko, F.: Palaeoenvironmental changes in the arid and sub arid belt (Sahara-Sahel-Arabian Peninsula) from 150 kyr to present, in: Past Climate Variability through Europe and Africa. Developments in Paleoenvironmental Research, edited by: Battarbee, R. W., Gasse, F., and Stickley, C. E., Springer, Dordrecht, 6, 219–256, https://doi.org/10.1007/978-1-4020-2121-3_12, 2007.

Hofmann, C., Courtillot, V., Féraud, G., Rochette, P., Yirgu, G., Ketefo, E., and Pik, R.: Timing of the Ethiopian flood basalt event and implications for plume birth and global change, Nature, 389, 838–841, https://doi.org/10.1038/39853, 1997.

Hooke, J. M.: 6.26 - River Meandering, in: Treatise on Geomorphology (Second Edition), edited by: Shroder, J. F., Academic Press, Oxford, 480–516, https://doi.org/10.1016/B978-0-12-409548-9.12517-5, 2022.

Huntley, D. and Baril, M.: The K content of the K-feldspars being measured in optical and thermoluminescence dating, Ancient TL, 15, 11–13, 1997.

Huntley, D. J. and Lamothe, M.: Ubiquity of anomalous fading in K-feldspars and the measurement and correction for it in optical dating, Can. J. Earth Sci., 38, 1093–1106, https://doi.org/10.1139/e01-013, 2001.

Japp, S., Gerlach, I., Hitgen, H., and Schnelle, M.: Yeha and Hawelti: cultural contacts between Saba' and D´MT – New research by the German Archaeological Institute in Ethiopia, Proc. Sem. Arab. Stud., 41, 145–160, 2011.

JAXA: ALOS Global Digital Surface Model (DSM) ALOS World 3D-30m (AW3D30) Ver. 2.2, JAXA – Japan Aerospace Exploration Agency [data set], https://www.eorc.jaxa.jp/ALOS/en/dataset/aw3d30/aw3d30_e.htm (last access: 17 January 2023), 2005.

Junge, A., Lomax, J., Shahack-Gross, R., Finkelstein, I., and Fuchs, M.: Chronology of an ancient water reservoir and the history of human activity in the Negev Highlands, Israel, Geoarchaeology, 33, 695–707, https://doi.org/10.1002/gea.21682, 2018.

Kennedy, D. M. and Woods, J. L. D.: 14.22 Determining Organic and Carbonate Content in Sediments, in: Treatise on Geomorphology, edited by: Shroder, J. F., Academic Press, San Diego, 262–273, https://doi.org/10.1016/B978-0-12-374739-6.00389-4, 2013.

Knox, J. C. and Daniels, J. M.: Watershed Scale and the Stratigraphic Record of Large Floods, in: Ancient Floods, Modern Hazards, 237–255, https://doi.org/10.1029/WS005p0237, 2002.

Korup, O.: 9.15 Landslides in the Fluvial System, in: Treatise on Geomorphology, edited by: Shroder, J. F., Academic Press, San Diego, 244–259, https://doi.org/10.1016/B978-0-12-374739-6.00240-2, 2013.

Krbetschek, M. R., Götze, J., Dietrich, A., and Trautmann, T.: Spectral information from minerals relevant for luminescence dating, Radiat. Meas., 27, 695–748, https://doi.org/10.1016/S1350-4487(97)00223-0, 1997.

Kreutzer, S., Schmidt, C., Fuchs, M. C., Dietze, M., Fischer, M., and Fuchs, M.: Introducing an R package for luminescence dating analysis, Ancient TL, 30, 1–8, 2012.

Kulig, G.: Erstellung einer Auswertesoftware zur Altersbestimmung mittels Lumineszenzverfahren unter spezieller Berücksichtigung des Einflusses radioaktiver Ungleichgewichte in der 238-U-Zerfallsreihe, Bakkalaureusarbeit Network Computing, TU Freiberg, unpublished thesis, 2005.

Lamb, H. F., Leng, M. J., Telford, R. J., Ayenew, T., and Umer, M.: Oxygen and carbon isotope composition of authigenic carbonate from an Ethiopian lake: a climate record of the last 2000 years, Holocene, 17, 517–526, https://doi.org/10.1177/0959683607076452, 2007a.

Lamb, H. F., Bates, C. R., Coombes, P. V., Marshall, M. H., Umer, M., Davies, S. J., and Dejen, E.: Late Pleistocene desiccation of Lake Tana, source of the Blue Nile, Quaternary Sci. Rev., 26, 287–299, https://doi.org/10.1016/j.quascirev.2006.11.020, 2007b.

Lamb, H. F., Bates, C. R., Bryant, C. L., Davies, S. J., Huws, D. G., Marshall, M. H., Roberts, H. M., and Toland, H.: 150,000-year palaeoclimate record from northern Ethiopia supports early, multiple dispersals of modern humans from Africa, Scientific Reports, 8, 1077, https://doi.org/10.1038/s41598-018-19601-w, 2018.

Lanckriet, S., Schwenninger, J.-L., Frankl, A., and Nyssen, J.: The Late-Holocene geomorphic history of the Ethiopian Highlands: Supportive evidence from May Tsimble, CATENA, 135, 290–303, https://doi.org/10.1016/j.catena.2015.08.011, 2015.

Leclant, J.: Haoulti-Melazo (1955–1956), Annales d'Ethiopie, 3, 43–82, 1959.

Lüthgens, C., Neuhuber, S., Grupe, S., Payer, T., Peresson, M., and Fiebig, M.: Geochronological investigations using a combination of luminescence and cosmogenic nuclide burial dating of drill cores from the Vienna Basin, Z. Dtsch. Ges. Geowiss., 168, 115–140, https://doi.org/10.1127/zdgg/2017/0081, 2017.

Machado, M.: Geomorphology of the Adwa District, in: Landscapes and Landforms of Ethiopia, World Geomorphological Landscapes, edited by: Billi, P., Springer, Dordrecht, 163–178, https://doi.org/10.1007/978-94-017-8026-1_8, 2015.

Machado, M. J., Pérez-González, A., and Benito, G.: Paleoenvironmental Changes during the Last 4000 yr in the Tigray, Northern Ethiopia, Quaternary Res., 49, 312–321, https://doi.org/10.1006/qres.1998.1965, 1998.

Marshall, M., Lamb, H., Davies, S., Leng, M., Bedaso, Z., Umer, M., and Bryant, C.: Climatic change in northern Ethiopia during the past 17,000 years: A diatom and stable isotope record from Lake Ashenge, Palaeogeogr. Palaeocl., 279, 114–127, https://doi.org/10.1016/j.palaeo.2009.05.003, 2009.

McGuire, C. and Rhodes, E. J.: Downstream MET-IRSL single-grain distributions in the Mojave River, southern California: Testing assumptions of a virtual velocity model, Quat. Geochronol., 30, 239–244, https://doi.org/10.1016/j.quageo.2015.02.004, 2015.

Mejdahl, V.: Thermoluminescence dating: beta attenuation in quartz grains, Archaeometry, 21, 61–72, https://doi.org/10.1111/j.1475-4754.1979.tb00241.x, 1979.

Menn, T. M.: Hawelti-Melazo: the French legacy and recent research – In memoriam Henri de Contenson (1926-2019), Annales d'Éthiopie, 33, 155–166, 2020.

Ménot, G., Pivot, S., Bouloubassi, I., Davtian, N., Hennekam, R., Bosch, D., Ducassou, E., Bard, E., Migeon, S., and Revel, M.: Timing and stepwise transitions of the African Humid Period from geochemical proxies in the Nile deep-sea fan sediments, Quaternary Sci. Rev., 228, 106071, https://doi.org/10.1016/j.quascirev.2019.106071, 2020.

Miall, A. D.: The geology of fluvial deposits: sedimentary facies, basin analysis, and petroleum geology, Springer, Berlin [u.a.], XVI, 582 pp., https://doi.org/10.1007/978-3-662-03237-4, 1996.

Moeyersons, J., Nyssen, J., Poesen, J., Deckers, J., and Haile, M.: Age and backfill/overfill stratigraphy of two tufa dams, Tigray Highlands, Ethiopia: Evidence for Late Pleistocene and Holocene wet conditions, Palaeogeogr. Palaeocl., 230, 165–181, https://doi.org/10.1016/j.palaeo.2005.07.013, 2006.

Nir, N., Knitter, D., Hardt, J., and Schütt, B.: Human movement and gully erosion: Investigating feedback mechanisms using Frequency Ratio and Least Cost Path analysis in Tigray, Ethiopia, PLoS ONE, 16, e0245248, https://doi.org/10.1371/journal.pone.0245248, 2021.

Nir, N., Stahlschmidt, M., Busch, R., Lüthgens, C., Schütt, B., and Hardt, J.: Footpaths: Pedogenic and geomorphological long-term effects of human trampling, CATENA, 215, 106312, https://doi.org/10.1016/j.catena.2022.106312, 2022.

Nyssen, J., Moeyersons, J., Poesen, J., Haile, M., and Deckers, J. A.: Argillipedoturbation and the development of rock fragment covers on Vertisols in the Ethiopian Highlands, BELGEO, 2, 183–194, https://doi.org/10.4000/belgeo.16184, 2002.

Nyssen, J., Poesen, J., Moeyersons, J., Deckers, J., Haile, M., and Lang, A.: Human impact on the environment in the Ethiopian and Eritrean highlands – a state of the art, Earth-Sci. Rev., 64, 273–320, https://doi.org/10.1016/S0012-8252(03)00078-3, 2004.

Nyssen, J., Poesen, J., Moeyersons, J., Deckers, J., and Haile, M.: Processes and rates of rock fragment displacement on cliffs and scree slopes in an *amba* landscape, Ethiopia, Geomorphology, 81, 265–275, https://doi.org/10.1016/j.geomorph.2006.04.021, 2006a.

Nyssen, J., Poesen, J., Veyret-Picot, M., Moeyersons, J., Haile, M., Deckers, J., Dewit, J., Naudts, J., Teka, K., and Govers, G.: Assessment of gully erosion rates through interviews and measurements: a case study from northern Ethiopia, Earth Surf. Proc. Land., 31, 167–185, https://doi.org/10.1002/esp.1317, 2006b.

Nyssen, J., Naudts, J., De Geyndt, K., Haile, M., Poesen, J., Moeyersons, J., and Deckers, J.: Soils and land use in the Tigray highlands (Northern Ethiopia), Land Degrad. Dev., 19, 257–274, https://doi.org/10.1002/ldr.840, 2008.

Nyssen, J., Frankl, A., Haile, M., Hurni, H., Descheemaeker, K., Crummey, D., Ritler, A., Portner, B., Nievergelt, B., Moeyersons, J., Munro, N., Deckers, J., Billi, P., and Poesen, J.: Environmental conditions and human drivers for changes to north Ethiopian mountain landscapes over 145 years, Sci. Total Environ., 485-486, 164–179, https://doi.org/10.1016/j.scitotenv.2014.03.052, 2014.

Pazzaglia, F. J.: 9.22 Fluvial Terraces, in: Treatise on Geomorphology, edited by: Shroder, J. F., Academic Press, San Diego, 379–412, https://doi.org/10.1016/B978-0-12-374739-6.00248-7, 2013.

Phillipson, D. W.: Foundations of an African civilisation: Aksum & the Northern Horn, 1000 BC – AD 1300, 1st edn., Eastern Africa series, Currey, Woodbridge, X, 293 pp., ISBN 9781846158735, 2012.

Pietsch, D. and Machado, M. J.: Colluvial deposits – proxies for climate change and cultural chronology. A case study from Tigray, Ethiopia, Z. Geomorphol, 58, 119–136, https://doi.org/10.1127/0372-8854/2012/S-00114, 2014.

Prescott, J. R. and Hutton, J. T.: Cosmic ray contributions to dose rates for luminescence and ESR dating: Large depths and long-term time variations, Radiat. Meas., 23, 497–500, https://doi.org/10.1016/1350-4487(94)90086-8, 1994.

Prescott, J. R. and Stephan, L. G.: The contribution of cosmic radiation to the environmental dose for thermoluminescence dating. Latitude, altitude and depth dependences, PACT, 6, 17–25, 1982.

Rades, E. F., Fiebig, M., and Lüthgens, C.: Luminescence dating of the Rissian type section in southern Germany as a base for correlation, Quatern. Int., 478, 38–50, https://doi.org/10.1016/j.quaint.2016.07.055, 2018.

Reeves, C. C. (Ed.): Chapter 6 Lacustrine Sediments: Clastic, in: Developments in Sedimentology, Elsevier, 77–85, https://doi.org/10.1016/S0070-4571(08)70829-X, 1968.

Reimer, P. J., Bard, E., Bayliss, A., Beck, J. W., Blackwell, P. G., Ramsey, C. B., Buck, C. E., Cheng, H., Edwards, R. L., Friedrich, M., Grootes, P. M., Guilderson, T. P., Haflidason, H., Hajdas, I., Hatte, C., Heaton, T. J., Hoffmann, D. L., Hogg, A. G., Hughen, K. A., Kaiser, K. F., Kromer, B., Manning, S. W., Niu, M., Reimer, R. W., Richards, D. A., Scott, E. M., Southon, J. R., Staff, R. A., Turney, C. S. M., and van der Plicht, J.: Intcal13 and Marine13 Radiocarbon Age Calibration Curves 0–50,000 Years Cal BP, Radiocarbon, 55, 1869–1887, 2013.

Revel, M., Ducassou, E., Grousset, F. E., Bernasconi, S. M., Migeon, S., Revillon, S., Mascle, J., Murat, A., Zaragosi, S., and Bosch, D.: 100,000 Years of African monsoon variability recorded in sediments of the Nile margin, Quaternary Sci. Rev., 29, 1342–1362, https://doi.org/10.1016/j.quascirev.2010.02.006, 2010.

Rhodes, E. J.: Optically Stimulated Luminescence Dating of Sediments over the Past 200,000 Years, Annu. Rev. Earth Pl. Sc., 39, 461–488, https://doi.org/10.1146/annurev-earth-040610-133425, 2011.

Sloss, C. R., Westaway, K. E., Hua, Q., and Murray-Wallace, C. V.: 14.30 An Introduction to Dating Techniques: A Guide for Geomorphologists, in: Treatise on Geomorphology, edited by: Shroder, J. F., Academic Press, San Diego, 346–369, https://doi.org/10.1016/B978-0-12-374739-6.00399-7, 2013.

Stoops, G.: Guidelines for Analysis and Description of Soil and Regolith Thin Sections, 2nd edn., Soil Science Society of America, Inc., https://doi.org/10.1002/9780891189763, 2020.

Tadesse, T.: Geological Map 1:25000 ND 37-6 Axum, Geological Survey of Ethiopia, 1999.

Thrasher, I. M., Mauz, B., Chiverrell, R. C., and Lang, A.: Luminescence dating of glaciofluvial deposits: A review, Earth-Sci. Rev., 97, 133–146, https://doi.org/10.1016/j.earscirev.2009.09.001, 2009.

Umer, M., Legesse, D., Gasse, F., Bonnefille, R., Lamb, H. F., Leng, M. J., and Lamb, A. A.: Late Quaternary climate changes in the Horn of Africa, in: Past Climate Variability through Europe and Africa, edited by: Battarbee, R. W., Gasse, F., and Stickley, C. E., Springer Netherlands, Dordrecht, 159–180, https://doi.org/10.1007/978-1-4020-2121-3_9, 2004.

Verrecchia, E. P. and Trombino, L.: Pedogenic Features, in: A Visual Atlas for Soil Micromorphologists, Springer International Publishing, Cham, 93–133, https://doi.org/10.1007/978-3-030-67806-7_4, 2021.

Wallinga, J., Murray, A., and Wintle, A.: The single-aliquot regenerative-dose (SAR) protocol applied to coarse-grain feldspar, Radiat. Meas., 32, 529–533, https://doi.org/10.1016/S1350-4487(00)00091-3, 2000.

Williams, M., Talbot, M., Aharon, P., Abdl Salaam, Y., Williams, F., and Inge Brendeland, K.: Abrupt return of the summer monsoon 15,000 years ago: new supporting evidence from the lower White Nile valley and Lake Albert, Quaternary Sci. Rev., 25, 2651–2665, https://doi.org/10.1016/j.quascirev.2005.07.019, 2006.

Zgłobicki, W., Poesen, J., De Geeter, S., Boardman, J., Gawrysiak, L., Golosov, V., Ionita, I., Niacsu, L., Rodzik, J., Stankoviansky, M., and Stolz, C.: Sunken lanes – Development and functions in landscapes, Earth-Sci. Rev., 221, 103757, https://doi.org/10.1016/j.earscirev.2021.103757, 2021.